

Electronic and Magnetic Structure of Infinite-layer NdNiO₂: Trace of Antiferromagnetic Metal

Zhao Liu,¹ Zhi Ren,² W. Zhu,² Z. F. Wang,¹ and Jinlong Yang^{3,*}

¹Hefei National Laboratory for Physical Sciences at the Microscale, CAS Key Laboratory of Strongly-Coupled Quantum Matter Physics, University of Science and Technology of China, Hefei, Anhui 230026, China

²Institute of Natural Sciences, Westlake Institute of Advanced Study and School of Science, Westlake University, Hangzhou 300024, China

³Hefei National Laboratory for Physical Sciences at the Microscale, Synergetic Innovation Center of Quantum Information and Quantum Physics, University of Science and Technology of China, Hefei, Anhui 230026, China

The recent discovery of Sr-doped infinite-layer nickelate NdNiO₂ [D. Li *et al.* Nature **572**, 624 (2019)] offers an exciting platform for investigating unconventional superconductivity in nickelate-based compounds. In this work, we present a first-principles calculations for the electronic and magnetic properties of undoped parent NdNiO₂. Intriguingly, we found that: 1) the paramagnetic phase has complex Fermi pockets with 3D characters near the Fermi level; 2) by including electron-electron interactions, 3d-electrons of Ni tend to form (π, π, π) antiferromagnetic ordering at low temperatures; 3) with moderate interaction strength, 5d-electrons of Nd contribute small Fermi pockets that could weaken the magnetic order akin to the self-doping effect. Our results provide a plausible interpretation for the experimentally observed resistivity minimum and Hall coefficient drop. Moreover, we elucidate that antiferromagnetic ordering in NdNiO₂ is relatively weak, arising from the small exchange coupling between 3d-electrons of Ni and also hybridization with 5d-electrons of Nd.

Since the discovery of high-temperature (high- T_c) superconductivity in cuprates¹, extensive effort has been devoted to investigate unconventional superconductors, ranging from non-oxide compounds^{2,3} to iron-based materials^{4,5}. Exploring high- T_c materials could provide a new platform to understand the fundamental physics behind high- T_c phenomenon, thus is quite valuable. Very recently, the discovery of superconductivity in Sr-doped NdNiO₂⁶ potentially raises the possibility to realize high- T_c in nickelate family^{7,8}.

One key experimental observation for the infinite-layer NdNiO₂ is that its resistivity exhibits a minimum around 70 K and an upturn at a lower temperature⁶. At the same time that the resistivity reaches minimum, the Hall coefficient drops towards a large value, signalling the loss of charge carriers⁶. Interestingly, no long-range magnetic order has been observed in powder neutron diffraction on NdNiO₂ when temperature is down to 1.7 K⁶. This greatly challenges the existing theories, since it is generally believed that magnetism holds the key to understand unconventional superconductivity⁹⁻¹². Therefore, it is highly desirable to study the magnetic properties of undoped parent NdNiO₂ and elucidate its experimental indications.

In this work, the electronic and magnetic properties of NdNiO₂ are systemically studied by first-principles calculations combined with classical Monte Carlo calculations. Firstly, the paramagnetic (PM) phase is studied. Its Fermi surface includes one large sheet and two electron pockets at Γ and A point, respectively. This can be described by a three-band low-energy effective model that captures the main physics of exchange coupling mechanism. Then, the magnetic properties are studied by including Hubbard U and (π, π, π) antiferromagnetic (AFM) ordering is confirmed to be the magnetic ground state. Most significantly, the Fermi surface of AFM phase is simpler than that of PM

phase, demonstrating an interaction induced elimination of Fermi pockets. Before NdNiO₂ enters correlated insulator, it is a compensated metal with one small electron pocket formed by d_{xy} orbital of Nd and four small hole pockets formed by d_{z^2} orbital of Ni. The estimated phase transition temperature (T_N) from PM phase to (π, π, π) AFM phase is 70 ~ 90 K for moderate interaction strength of $U = 5 \sim 6$ eV.

Through these studies, we identify two key messages that are distinguishable from the cuprates: 1) NdNiO₂ is dominated by the physics of Mott-Hubbard instead of charge-transfer; 2) effective exchange coupling parameters are about one-order smaller than those of cuprates. In this regarding, supposed that the ground state is magnetic, our calculations demonstrate (π, π, π) AFM ordering is energetically favorable. Moreover, our results provide a natural understanding of two experimental observations. First, 3d-electrons of Ni tend to form AFM ordering around 70 ~ 90 K, coinciding with the minimum in resistivity and the drop in Hall coefficient. Second, the (π, π, π) AFM ordering could be weak (compared with cuprates), because of the small effective exchange coupling and the hybridization with itinerant 5d-electrons of Nd. This could be the reason why AFM ordering is missing in previous study, which calls for more careful neutron scattering measurements on NdNiO₂.

The first-principle calculations are carried out with the plane wave projector augmented wave method as implemented in the Vienna *ab initio* simulations package (VASP)¹³⁻¹⁵. The Perdew-Burke-Ernzerhof (PBE) functionals of generalized gradient approximation (GGA) is used for PM phase¹⁶. To incorporate the electron-electron interactions, DFT + U is used for AFM phase, which can reproduce correctly the gross features of correlated-electrons in transition metal oxides¹⁷⁻¹⁹. The 4f electrons of Nd³⁺

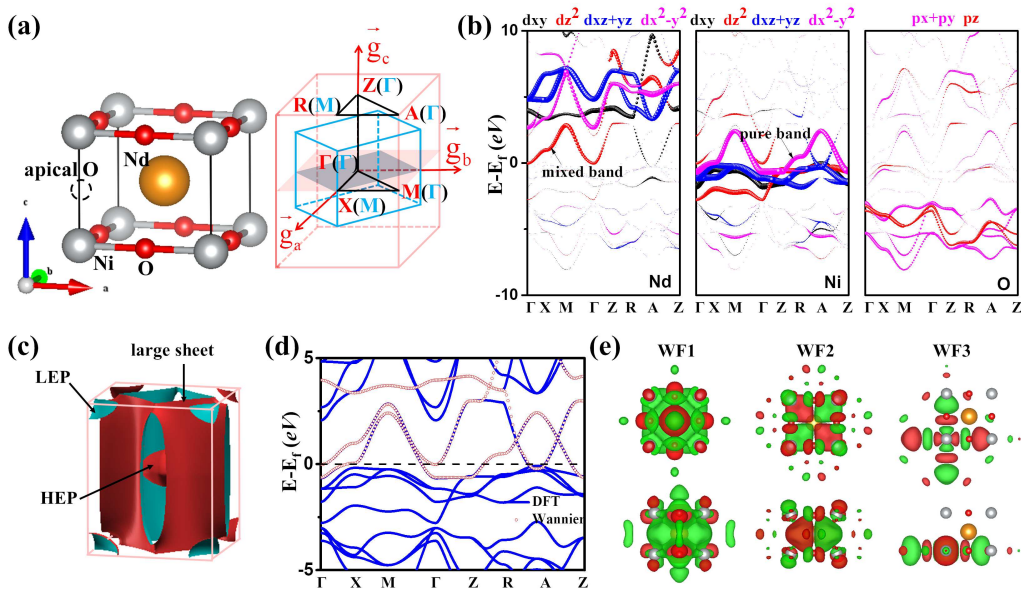


Figure 1: (a) Atomic structure of tetragonal NdNiO₂ and first Brillouin zone. The red and blue lines (labels) denotes the first Brillouin zone of PM phase and (π, π, π) AFM phase, respectively. The high symmetric line for band calculation are $\Gamma(0, 0, 0)$ -X(0.5, 0, 0)-M(0.5, 0.5, 0)- Γ -Z(0, 0, 0.5)-R(0.5, 0, 0.5)-A(0.5, 0.5, 0.5)-Z. (b) Orbital resolved band structure of PM phase. The d_{xy} , d_{z^2} , d_{xz+yz} and $d_{x^2-y^2}$ of Nd (spin-up Ni, spin-down Ni) are marked by black, red, blue and pick filled circles. The p_z and p_{x+y} of O are marked by red, blue and pick filled circles. The size of circles represents the orbital weights. (c) Perspective view of Fermi surfaces. LEP and HEP denotes light and heavy electron pocket, respectively. (d) The comparison between first-principles and Wannier-fitting bands around the Fermi-level. (e) Top and side view of three maximally localized Wannier functions.

are expected to display the local magnetic moment as Nd³⁺ in Nd₂CuO₄²⁰ and are treated as the core-level electrons. The Hubbard U ($0 \sim 8$ eV) term is added to $3d$ electrons of Ni. The energy cut-off of 600 eV, and Monkhorst-Pack k point mesh of $11 \times 11 \times 11$ and $18 \times 18 \times 30$ is used for PM and AFM phase, respectively. The maximally localized Wannier functions (WFs) are constructed by using Wannier90 package^{23,24}. The structure of infinite-layer NdNiO₂ is shown in Fig. 1(a), including NiO₂ layers sandwiched by Nd, which can be obtained from the perovskite NdNiO₃ with reduction of apical O atoms in c direction^{21,22}. Due to apical O vacancies, the lattice constant in c direction shrinks (smaller than a direction) and the space group becomes $P4/mmm$. The experimental lattice constant $a = b = 3.92$ Å and $c = 3.28$ Å are used in our calculations.

Firstly, We present the band structure of PM phase without Hubbard U . The orbital resolved band structure of PM phase is shown in Fig. 1(b). Comparing with typical cuprates CaCuO₂²⁵, two significant differences are noted: 1) there is a gap ~ 2.5 eV between $2p$ orbitals of O and $3d$ orbitals of Ni. According to Zaanen-Sawatzky-Allen classification scheme²⁶, this indicates that the physics of NdNiO₂ is close to Mott-Hubbard rather than charge-transfer; 2) there are two bands crossing the Fermi level, in which one is mainly contributed by $d_{x^2-y^2}$ orbital of Ni (called pure-band) and the other one has a complicated orbital compositions (called mixed-band). In $k_z = 0$ plane, the mixed-band is mainly contributed by d_{z^2} orbital of Nd and

Ni. The dispersion around Γ point is relatively small, called heavy electron pocket (HEP). In $k_z = 0.5$ plane, the mixed-band is mainly contributed by d_{xy} (d_{xz} , d_{yz} and d_{z^2}) orbital of Nd (Ni). The dispersion around A point is relatively large, called light electron pocket (LEP). As a comparison, one notices that there is only one pure-band crossing the Fermi level in CaCuO₂²⁵. The Fermi surface of PM phase is shown in Fig. 1(c). There is a large sheet contributed by the pure-band, as the case in CaCuO₂²⁵. This Fermi surface is obviously two-dimensional (2D), because of the weak dispersion along Γ -Z. In addition, there are two electron pockets residing at Γ and A point, respectively, showing a feature of three-dimensional (3D) rather than 2D (see labels HEP and LEP in Fig. 1(c)). Therefore, the 3D metallic state will be hybridized with the 2D correlated state in NiO₂ plane, suggesting NdNiO₂ to be an "oxide-intermetallic" compound^{27,28}.

The existence of mixed-band also reflects the inherent interactions between Nd $5d$ and Ni $3d$ electrons. To explore the low energy physics of NdNiO₂, a three-band model consisting of Ni $d_{x^2-y^2}$, Nd d_{z^2} and Nd d_{xy} orbitals is constructed by Wannier90 package. As shown Fig. 1(d), one can see the good agreement between first-principles and Wannier-fitting bands near the Fermi level. The corresponding three maximally localized WFs are shown in Fig. 1(e), demonstrating the main feature of d_{z^2} (WF1) and d_{xy} (WF2) orbital of Nd, and $d_{x^2-y^2}$ (WF3) orbital of Ni. However, these WFs still have some derivations from standard atomic orbitals, that is, WF1 and WF2 are mixed

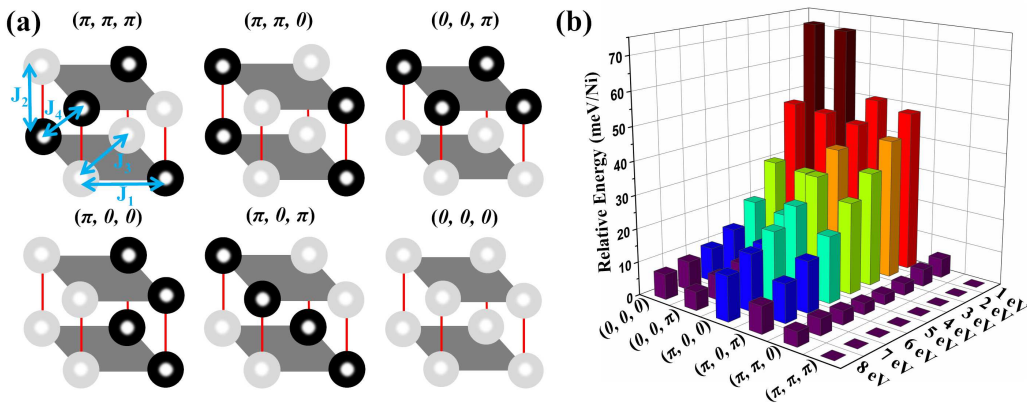


Figure 2: (a) Illustration of six collinear spin configurations. The white and black ball represents local up and down spin moment, respectively. The four exchange coupling parameters are indicated by the blue arrows. (b) Energy comparison for the six collinear spin configurations with different values of Hubbard U . Energy of (π, π, π) AFM is set to zero.

with d_{z^2} orbital of Ni, and WF3 is mixed with $p_{x/y}$ orbital of O in the NiO_2 plane. According to the classical Goodenough-Kanamori-Anderson rules²⁹⁻³¹, these derivations (or hybridizations) will give clues for the magnetic properties.

To determine the magnetic ground state of NdNiO_2 , six collinear spin configurations are taken into account in a $2 \times 2 \times 2$ supercell, that is, AFM1 with $\mathbf{q} = (\pi, \pi, \pi)$, AFM2 with $\mathbf{q} = (\pi, \pi, 0)$, AFM3 with $\mathbf{q} = (0, 0, \pi)$, AFM4 with $\mathbf{q} = (\pi, 0, 0)$, AFM5 with $\mathbf{q} = (\pi, 0, \pi)$ and FM with $\mathbf{q} = (0, 0, 0)$, as shown in Fig. 2(a). Within all Hubbard U ranges, we found that AFM1 configuration always has the lowest energy, as shown in Fig. 2(b), indicating a stable (π, π, π) AFM phase with respect to electron-electron interactions and is in accordance with random phase approximation treatment³². This can be attributed to the special orbital distributions around the Fermi level. The intralayer NN exchange coupling is the typical 180° typed Ni-O-Ni superexchange coupling, that is, the coupling between $d_{x^2-y^2}$ orbital of Ni is mediated by $p_{x/y}$ orbital of O (see WF3), preferring a (π, π) AFM phase in NiO_2 plane. The interlayer NN exchange coupling is due to the superexchange between the Ni d_{z^2} orbitals mediated by Nd d_{z^2} orbital as shown in WF1, preferring a (π, π) AFM phase between NiO_2 planes. Therefore, the superexchange coupling results in a stable (π, π, π) AFM phase in NdNiO_2 . Moreover, the magnetic anisotropy is further checked by including the spin-orbit coupling (SOC). We found that the spin moment prefers along c direction with the magnetic anisotropic energy of ~ 0.5 meV/Ni. Thus, the tiny SOC effect can be safely neglected in the following phase transition temperature calculations.

In cuprates, the Fermi surface is unstable with electron-electron interactions, making its parent phase to be an AFM insulator. However, this is apparently not the case in NdNiO_2 , because of the extra electron pockets and the inherent interaction between Nd $5d$ and Ni $3d$ electrons. At $U=0$ eV, there are two electron pockets at Γ point and two hole pockets along X-R direction as shown in Fig. 3(a)-(b). Physically,

the origin of these four pockets can be easily understood through the comparison of orbital resolved band structures between PM phase (Fig. 1(b)) and (π, π, π) AFM phase (Fig. 4). Because of the Zeeman field on Ni, its spin-up and -down bands are split away from each other. The original pure-band ($d_{x^2-y^2}$ orbital of Ni) in PM phase becomes partially occupied in spin-up channel (forming two hole pockets) and totally unoccupied in spin-down channel. Hence, the two hole pockets in AFM phase are inherited from large sheet in PM phase, showing a 2D character with neglectable dispersion along Γ -Z direction. For the electron pockets at Γ point, the heavier one is mainly contributed by d_{z^2} orbital of Nd and Ni, so it comes from the HEP at Γ point of PM phase. While for the lighter one, it comes from the LEP at A point of PM phase which is folded into the Γ point of (π, π, π) AFM phase [see Fig. 1(a)]. The orbital composition can also be used to check this folded band, which is contributed by d_{xy} orbital of Nd, $d_{xz/yz}$ (d_{z^2}) orbital of spin-down (-up) Ni.

These pockets have a different evolution with the increasing value of Hubbard U . For electron pockets, the heavier one is very sensitive to Hubbard U and disappears at $U = 1$ eV. Meanwhile the lighter one doesn't appear until $U = 6$ eV. In addition, the orbital components of lighter electron pockets are purified by electron-electron interaction and it mainly contributed by d_{xy} of Nd in the large U limit as shown in Fig. 4. The case for hole pockets is rather complicated. Firstly, the bands of hole pockets become flat with the increasing value of Hubbard U . Secondly, the original hole pockets formed by $d_{x^2-y^2}$ orbital of Ni gradually disappear, meanwhile, a new hole pocket formed by d_{z^2} orbital of Ni appears along Γ -M as shown in Fig. 3(d). At $U = 6$ eV, NdNiO_2 is a compensated metal with a small electron pocket at Γ point and four hole pockets along Γ -M as displayed in Fig. 3(e). Further increasing the value of Hubbard U , the system enters an AFM insulator, just like cuprates. Therefore, the metal-to-insulator phase transition point is near $U \sim 6$ eV. If Hubbard U is less than 6 eV, NdNiO_2 is an AFM

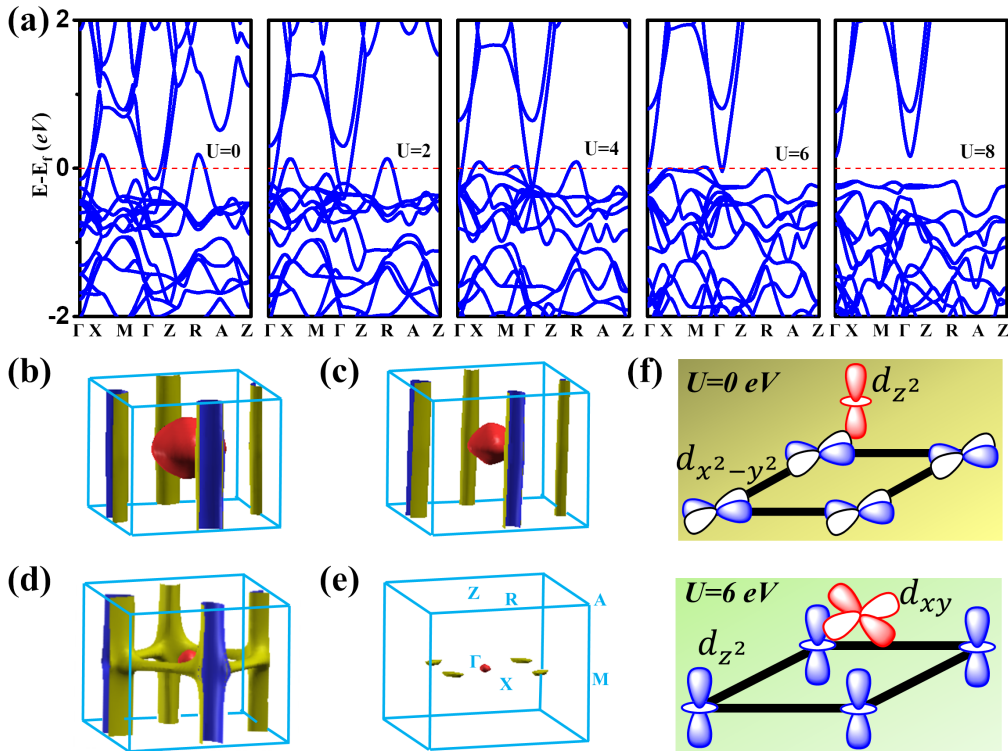


Figure 3: (a) Band structures of (π, π, π) AFM phase with different values of Hubbard U . (b)-(e) Perspective view of the Fermi surfaces of (π, π, π) AFM with $U = 0, 2, 4, 6$ eV. The two hole pockets in (b)-(d) are degenerated and can not be distinguished from this picture. The high symmetry k -points in (e) are labelled to guide the eye. (f) Schematic diagram of major self-doping channel at $U = 0$ and $U = 6$ eV. The red/blue color represents d orbital of Nd/Ni respectively.

metal with relatively small amount of holes that are self-doped^{27,32-35} into d orbitals of Ni. Interestingly, there is an orbital shift from $3d_{x^2-y^2}$ orbital of Ni at $U = 0$ eV to $3d_{z^2}$ orbital of Ni at $U = 6$ eV in the NiO₂ plane, as depicted in Fig. 3(f). We speculate that this orbital shift may change the paradigm after doping^{8,36}. Moreover, without the Hubbard U , the $2p$ orbital of O is far away from the Fermi level, just like the case of PM phase. However, with the increasing value of Hubbard U , the gap between $3d$ orbital of Ni and $2p$ orbital of O gradually decreases (Fig. 4), demonstrating an evolution from Mott-Hubbard metal to charge-transfer insulator.

In order to quantitatively describe such a phenomenon, the phase transition temperature is further calculated. For (π, π, π) AFM phase, the magnetic momentum of Ni increases from $0.58 \mu_B$ ($U = 0$ eV) to $1.04 \mu_B$ ($U = 8$ eV) and becomes gradually saturated, as shown in Fig. 5(a). This is also consistent with the fact that $d_{x^2-y^2}$ orbital of Ni is closer to single occupation with the increasing value of Hubbard U . Therefore, Ni is spin one half ($S = 1/2$) in infinite-layer NdNiO₂, just like the case in cuprates. To extract the exchange coupling parameters of J_1, J_2, J_3 and J_4 (as labelled in Fig. 2(a)), the total energy of five AFM configurations obtained from DFT + U calculations are mapped onto the Heisenberg spin Hamiltonian. In the $2 \times 2 \times 2$ supercell, there are 8 Ni atoms and the total energy of different AFM configurations are:

$$\begin{aligned}
 E_{\text{AFM1}} &= E_0 - 16J_1S^2 - 8J_2S^2 + 16J_3S^2 + 32J_4S^2 \\
 E_{\text{AFM2}} &= E_0 - 16J_1S^2 + 8J_2S^2 + 16J_3S^2 - 32J_4S^2 \\
 E_{\text{AFM3}} &= E_0 + 16J_1S^2 - 8J_2S^2 + 16J_3S^2 - 32J_4S^2 \\
 E_{\text{AFM4}} &= E_0 + 8J_2S^2 - 16J_3S^2 + 32J_4S^2 \\
 E_{\text{AFM5}} &= E_0 - 8J_2S^2 - 16J_3S^2 - 32J_4S^2
 \end{aligned} \quad (1)$$

where E_0 is the reference energy without magnetic order. The calculated exchange coupling parameters as a function of Hubbard U are shown in Fig. 5(b). We would like to make several remarks here: 1) the NN intralayer exchange coupling (J_1), mediated by $d_{x^2-y^2}$ orbital of Ni, demonstrates a $1/U$ law; 2) the NN interlayer exchange coupling (J_2) is ~ 10 meV with little variation. The positive value of J_2 indicates an AFM coupling between NiO₂ planes; 3) the next NN intralayer exchange coupling (J_3), mediated by d_{xy} orbital of Nd, is comparable to J_1 at large value of Hubbard U , which is dramatically different to that in infinite-layer SrFeO₂³⁷⁻³⁹. This large value could be attributed to the relative robustness of lighter electron pocket and orbital purification; 4) the next NN interlayer exchange coupling (J_4) is ~ 0 meV, indicating the validity of our Hamiltonian up to the third NN; 5) J_1, J_2 and J_3 have the same strength at large U , suggesting NdNiO₂ is a 3D magnet rather than 2D magnet.

Based on the above exchange coupling parameters, the phase transition temperature (T_N) is calculated by

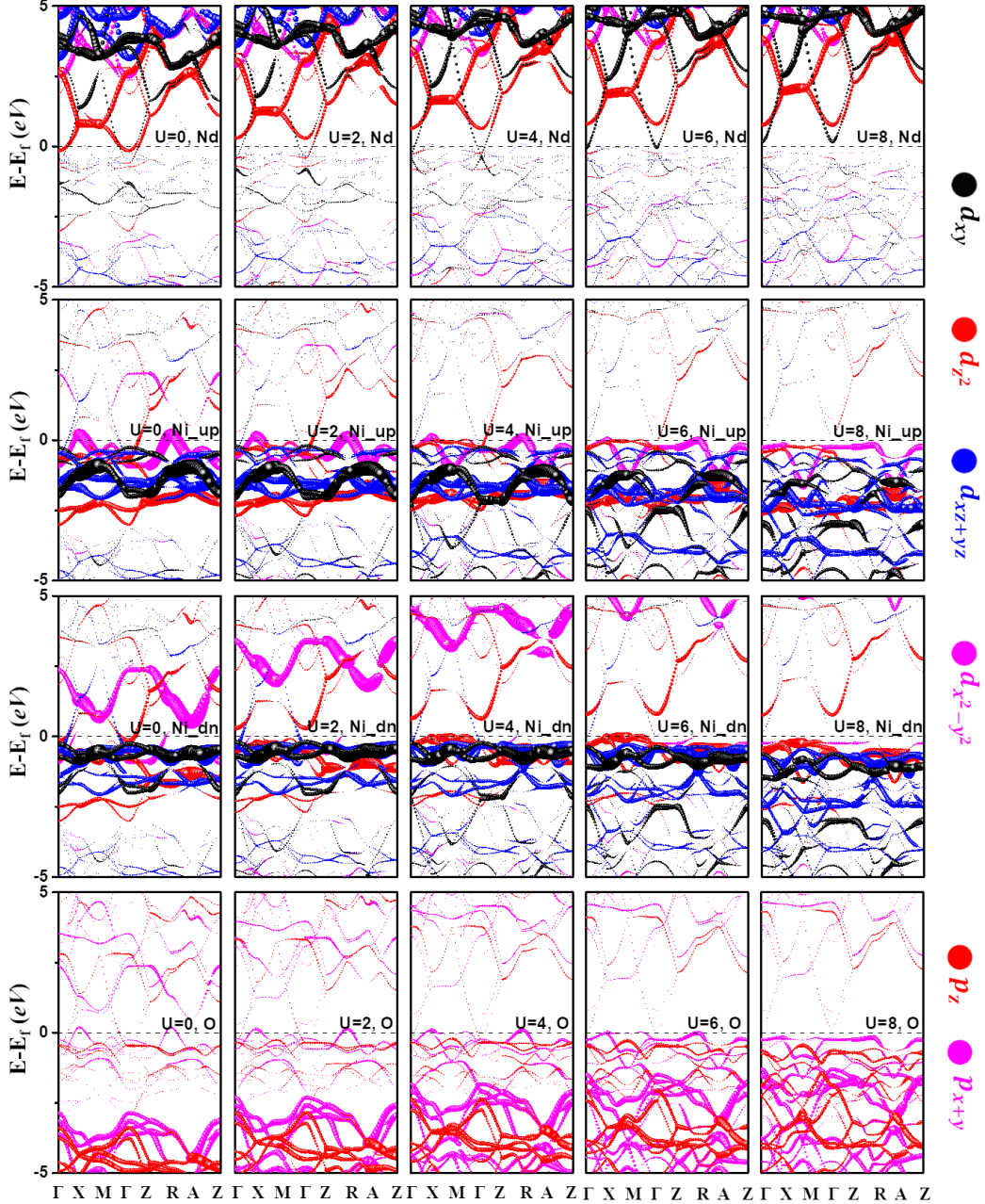


Figure 4: Orbital resolved band structures of (π, π, π) AFM phase with different values of Hubbard- U . The first, second, third and fourth row represents Nd, spin-up Ni, spin-down Ni and O, respectively. The filled circles with different colors have the same meaning as those in Fig. 1. The name of d orbitals in the AFM supercell has been aligned to that of unit cell.

classical Monte Carlo method in a $12 \times 12 \times 12$ supercell based on the classical spin Hamiltonian:

$$H = \sum_{\langle i,j \rangle} J_{ij} \vec{S}_i \cdot \vec{S}_j \quad (2)$$

where the spin exchange parameters J_{ij} have been defined above. First, we calculate the specific heat (C) after the system reaches equilibrium at a each given temperature (T), as shown in Fig. 5(c). Then, T_N is extracted from the peak position in the curve of $C(T)$, as shown in Fig. 5(c). For $U = 1$ eV, T_N is as high as

220 K, which can be ascribed to the large value of J_1 . With the increasing value of Hubbard U , T_N gradually decreases and becomes ~ 70 K at $U = 6$ eV. To further check the effect of interlayer exchange coupling on 3D magnet, an additional Monte Carlo calculation is performed without J_2 and J_4 . As shown in Fig. 5(e), the $C(T)$ vs T plot shows a broaden peak at a lower temperature. Since Mermin-Wagner theorem prohibit magnetic order in 2D isotropic Heisenberg model at any nonzero temperatures⁴⁰, the broad peak in $C(T)$ vs T plot implies the presence of short-range order.

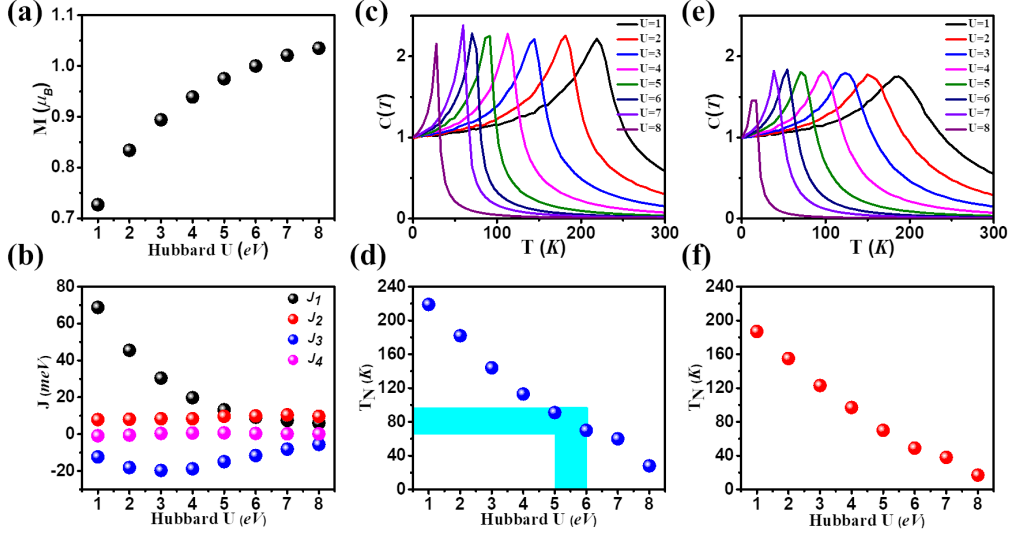


Figure 5: The Hubbard U dependence of (a) the magnetic momentum of Ni in (π, π, π) AFM phase, (b) the exchange coupling parameters, (c) specific heat (C) vs T with four J 's, (d) the estimated T_N with four J 's, (e) specific heat (C) vs T with J_1, J_3 only and (f) the estimated T_N with J_1, J_3 only. The shaded region in (d) highlights the possible T_N of $70 \sim 90$ K with a reasonable $U = 5 \sim 6$ eV.

Regarding the small drop of T_N (about 30 K in Fig. 5(f)), our MC simulations indicate that the weak interactions between NiO_2 planes.

Although the exact value of Hubbard U cannot be directly extracted from the first principles calculations, its value range can still be estimated based on similar compounds. The infinite-layer nickelates are undoubtedly worse metals compared to elemental nickel with $U \sim 3$ eV⁴¹, which can be considered as a lower bound of Hubbard U . The Coulomb interaction in infinite-layer nickelates should be smaller than that in the charge-transfer insulator NiO with $U \sim 8$ eV¹⁷, which can be considered as an upper bound of Hubbard U . Therefore, a reasonable value of Hubbard U in NdNiO_2 will be between 3 eV and 8 eV. In the following discussions, we use $U = 5 \sim 6$ eV^{27,42} to draw our conclusions: 1) with the decreasing of temperature, there is a phase transition from PM phase to (π, π, π) AFM phase near $70 \sim 90$ K; 2) the exchange-coupling parameters are ~ 10 meV, which is one order smaller than cuprates⁴³⁻⁴⁷ and results in a low T_N compared with cuprates; 3) the self-doing effect from $5d$ orbital of Nd and $3d$ orbital of Ni may screen the local magnetic momentum in $d_{x^2-y^2}$ orbital of Ni, which gives a small magnetic momentum less than $1 \mu_B$ and makes the long-range AFM order unstable^{6,21,22,48}; 4) the Fermi surface of PM phase is quite large with two 3D-like electron pockets, while the Fermi surface of (π, π, π) AFM phase is quite small with one 3D-like electron pocket and four 2D-like hole pocket. Therefore, there could exist a crossover from normal metal to bad AFM metal around $T_N \sim 70 - 90$ K, which provides a plausible understanding of minimum of resistivity and Hall co-

efficient drop in infinite-layer NdNiO_2 ⁶. We envision that our calculations will intrigue intensive interests for studying the magnetic properties of high quality infinite-layer NdNiO_2 samples.

Lastly, we would like to make some remarks on the existing experiments. Some recent experiments fail to find bulk superconductivity in NdNiO_2 systems, and the parent samples show strong insulating behaviors⁴⁹. The insulating behavior could be attributed to strong inhomogeneous disorder or improper introduction of H during the reaction with CaH_2 ⁵⁰. Especially, it is worth noting, the experiments cannot rule out the possibility of weak AFM ordering, due to the presence of Ni impurities in their samples. (Actually this problem has been pointed out before^{21,22}.) The strong ferromagnetic order from elemental Ni would dominate over and wash out the weak signal of AFM ordering from NdNiO_2 as we suggested in this work. In this regard, the upcoming inelastic neutron scattering on high-quality samples is highly desired.

W.Z. thanks Chao Cao for sharing their unpublished DMFT results, and thanks Filip Ronning, H. H. Wen, G. M. Zhang for helpful discussion. This work was supported by NSFC (No. 11774325, 21603210, 21603205, 21688102), National Key Research and Development Program of China (No. 2017YFA0204904, 2016YFA0200604), Anhui Initiative in Quantum Information Technologies (No. AHY090400), Fundamental Research Funds for the Central Universities and the Start-up Funding from Westlake University. We thank Supercomputing Center at USTC for providing the computing resources.

* E-mail: jlyang@ustc.edu.cn

¹ J. G. Bednorz and K. A. Müller, Z. Phys. B **64**, 189-193

- (1986).
- ² J. Nagamatsu, N. Nakagawa, T. Muranaka, Y. Zenitani and J. Akimitsu, *Nature* **410**, 63-64 (2001).
 - ³ A. P. Drozdov, M. I. Eremets, I. A. Troyan, V. Ksenofontov and S. I. Shylin, *Nature* **525**, 73-76 (2015).
 - ⁴ Y. Kamihara, H. Hiramatsu, M. Hirano, R. Kawamura, H. Yanagi, T. Kamiya and H. Hosono, *J. Am. Chem. Soc.* **128**, 10012-10013 (2006).
 - ⁵ Q.-Y. Wang *et al.*, *Chin. Phys. Lett.* **29**, 037402 (2012).
 - ⁶ D. Li *et al.*, *Nature* **572**, 624-627 (2019).
 - ⁷ V. I. Anisimov, D. Bukhvalov and T. M. Rice, *Phys. Rev. B* **59**, 7901-7906 (1999).
 - ⁸ K.-W. Lee and W. E. Pickett, *Phys. Rev. B* **70**, 165109 (2004).
 - ⁹ A. L. Patrick, N. Nagaosa and X.-G. Wen, *Rev. Mod. Phys.* **78**, 17-85 (2006).
 - ¹⁰ B. Keimer, S. A. Kivelson, M. R. Norman, S. Uchida and J. Zaanen, *Nature* **518**, 179-186 (2015).
 - ¹¹ P. Dai, J. Hu and E. Dagotto, *Nat. Phys.* **8**, 709-718 (2012).
 - ¹² P. Dai, *Rev. Mod. Phys.* **87**, 855-896 (2015).
 - ¹³ M. P. Teter, M. C. Payne and D. C. Allan, *Phys. Rev. B* **40**, 12255 (1989).
 - ¹⁴ G. Kresse and J. Furthmüller, *Phys. Rev. B* **54**, 11169 (1996).
 - ¹⁵ P. E. Blöchl, *Phys. Rev. B* **50**, 17953 (1994).
 - ¹⁶ J. P. Perdew, K. Burke and M. Ernzerhof, *Phys. Rev. Lett.* **77**, 3865-3868 (1996).
 - ¹⁷ V. I. Anisimov, J. Zaanen and O. K. Anderson, *Phys. Rev. B* **44**, 943-954 (1991).
 - ¹⁸ S. L. Dudarev, G. A. Botton, S. Y. Savrasov, C. J. Humphreys and A. P. Sutton, *Phys. Rev. B* **57**, 1505 (1998).
 - ¹⁹ A. Rohrbach, J. Hafner and G. Kresse, *J. Phys.: Condens. Matter* **15**, 979-996 (2003).
 - ²⁰ H. Casalta, P. Bourges, M. d'Astuto, D. Petitgrand and A. Ivanov, *Phys. Rev. B* **57**, 471-475 (1998).
 - ²¹ M. A. Hayward, M. A. Green, M. J. Rosseinsky and J. Sloan, *J. Am. Chem. Soc.* **121**, 8843-8854 (1999).
 - ²² M. A. Hayward and M. J. Rosseinsky, *Solid State Sci.* **5**, 839-850 (2003).
 - ²³ A. A. Mostofi, J. R. Yates, Y.-S. Lee, I. Souza, D. Vanderbilt and N. Marzari, *Comput. Phys. Commun.* **178**, 685 (2008).
 - ²⁴ N. Marzari, A. A. Mostofi, J. R. Yates, I. Souza and D. Vanderbilt, *Rev. Mod. Phys.* **84**, 1419-1475 (2012).
 - ²⁵ A. S. Botana and M. R. Norman, arXiv: 1908.10946 (2019).
 - ²⁶ J. Zaanen, G. A. Sawatzky and J. W. Allen, *Phys. Rev. Lett.* **55**, 418-421 (1985).
 - ²⁷ M. Hepting *et al.*, arXiv: 1909.02678 (2019).
 - ²⁸ Y. Gu, S. Zhu, X. Wang, J. Hu and H. Chen, arXiv: 1911.00814 (2019).
 - ²⁹ J. B. Goodenough, *Phys. Rev.* **100**, 564 (1955).
 - ³⁰ P. W. Anderson, *Phys. Rev.* **115**, 2 (1959).
 - ³¹ J. Kanamori, *J. Phys. Chem. Solids* **10**, 87-89 (1959).
 - ³² X. Wu, D. Di Sante, T. Schwemmer, W. Hanke, H. Y. Hwang, S. Raghu and R. Thomale, arXiv: 1909.03015 (2019).
 - ³³ Y. Nomura, M. Hirayama, T. Tadano, Y. Yoshimoto, K. Nakamura and R. Arita, arXiv: 1909.03942 (2019).
 - ³⁴ H. Sakakibara, H. Usui, K. Suzuki, T. Kotani, H. Aoki, and K. Kuroki, arXiv: 1909.00060 (2019).
 - ³⁵ G.-M. Zhang, Y.-F. Yang and F.-C. Zhang, arXiv: 1909.11845 (2019).
 - ³⁶ F. Lechermann, arXiv: 1911.11521 (2019).
 - ³⁷ Y. Tsujimoto *et al.*, *Nature* **450**, 1062 (2007).
 - ³⁸ M. A. Hayward and M. J. Rosseinsky, *Nature* **450**, 960 (2007).
 - ³⁹ H. J. Xiang, S.-H. Wei and M.-H. Whangbo, *Phys. Rev. Lett.* **100**, 167207 (2008).
 - ⁴⁰ N. D. Mermin and H. Wagner, *Phys. Rev. Lett.* **100**, 1133-1136 (1966).
 - ⁴¹ F. Aryasetiawan, K. Karlsson, O. Jepsen and U. Schönberger, *Phys. Rev. B* **74**, 125106 (2006).
 - ⁴² M. Cococcioni and S. de Gironcoli, *Phys. Rev. B* **17**, 1133 (1966).
 - ⁴³ P. Bourges, H. Casalta, A. S. Ivanov and D. Petitgrand, *Phys. Rev. Lett.* **79**, 4906 (1997).
 - ⁴⁴ R. Coldea, S. M. Hayden, G. Aeppli, T. G. Perring, C. D. Frost, T. E. Mason, S.-W. Cheong and Z. Fisk, *Phys. Rev. Lett.* **86**, 5377 (2001).
 - ⁴⁵ L. Braicovich *et al.*, *Phys. Rev. Lett.* **102**, 167401 (2009).
 - ⁴⁶ G. Blumberg, R. Liu, M. V. Klein, W. C. Lee, D. M. Ginsberg, C. Gu, B. W. Veal and B. Dabrowski, *Phys. Rev. B* **49**, 13295 (1994).
 - ⁴⁷ G. Blumberg, P. Abbamonte, M. V. Klein, W. C. Lee, D. M. Ginsberg, L. L. Miller and A. Zibold, *Phys. Rev. B* **53**, R11930 (1994).
 - ⁴⁸ Y. Fu *et al.*, arXiv: 1911.03177 (2019).
 - ⁴⁹ Q. Li, C. He, S. Jin, X. Zhu, Y. Zhang and H.-H. Wen, arXiv: 1911.02420 (2019).
 - ⁵⁰ L. Si, W. Xiao, J. Kaufmann, J. M. Tomczak, Y. Lu, Z. Zhong and K. Held, arXiv: 1911.06917 (2019).